



# Enhanced photocatalytic oxidation of propylene over V-doped TiO<sub>2</sub> photocatalyst: Reaction mechanism between V<sup>5+</sup> and single-electron-trapped oxygen vacancy

Fengzhu Ren <sup>a</sup>, Haiyan Li <sup>b,c</sup>, Yuanxu Wang <sup>a,\*</sup>, Jianjun Yang <sup>b,\*\*</sup>

<sup>a</sup> Institute for Computational Materials Science, School of Physics and Electronics, Henan University, Kaifeng 475004, China

<sup>b</sup> Key Laboratory for Special Functional Materials, Henan University, Kaifeng 475004, China

<sup>c</sup> College of Chemistry and Chemical Engineering, Henan University, Kaifeng 475004, China

## ARTICLE INFO

### Article history:

Received 21 January 2015

Received in revised form 25 March 2015

Accepted 29 March 2015

Available online 31 March 2015

### Keywords:

Photocatalysis

Single-electron-trapped oxygen vacancy

V-doped TiO<sub>2</sub>

## ABSTRACT

The novel V-doped TiO<sub>2</sub> (V-TiO<sub>2</sub>[NTA]) samples with different (0–10%) concentration have been successfully prepared by a facile solid state sintering method using the nanotubular titanic acid (NTA) as titanium precursor for the first time, which shows remarkable photocatalytic activity for degradation of propylene under visible-light irradiation. Based on the density function theory (DFT) calculations in conjunction with a series of experimental characterization techniques including Raman spectra, TEM, XPS, ESR, and UV-vis DRS, a new V<sup>4+</sup> ions formation mechanism by means of the electron trapped at single-electron-trapped oxygen vacancy (SETOV, V<sub>o</sub><sup>•</sup>) not Ti<sup>3+</sup> has been proposed, and the origin of the observed remarkable improved photocatalytic activity of the V-TiO<sub>2</sub>[NTA] samples has also been investigated. At low concentration, the enhancement of photocatalytic activity for the V-TiO<sub>2</sub>[NTA] samples firstly come from the synergistic effect of V and V<sub>o</sub><sup>•</sup> co-doping: a part of V<sup>5+</sup> is reduced to V<sup>4+</sup> by V<sub>o</sub><sup>•</sup> into TiO<sub>2</sub> lattice, others exist on the surface in the form of V<sub>2</sub>O<sub>5</sub>. The incorporation of V<sup>4+</sup> in TiO<sub>2</sub> lattice induces some new states (around the top of the valence band, due to O 2p and V 3d orbitals; around the bottom of the conduction band, due to Ti 3d, O 2p, and V 3d orbitals) near the edge of the valence and conduction bands, respectively, causing an effective narrowing of the band gap. The narrowing of gap is responsible for the red-shifted and increased light-absorption. The presence of V<sup>5+</sup>/V<sup>4+</sup> redox couple facilitates the efficient separation and migration of photo-induced e<sup>-</sup>/h<sup>+</sup> pairs to generate active species. Secondly, the enhancement of photocatalytic activity with low doping concentration may also be ascribed to the increased surface area. At high doping concentration, the reasons for the decreased photocatalytic activity is that the same trapping sites may act as the recombination centers and excess V dopant may occupy the active sites of surface.

© 2015 Elsevier B.V. All rights reserved.

## 1. Introduction

Semiconductor photocatalysis has been considered to be a promising technique for solving current more and more serious energy and environmental problem [1–3]. Many researchers have proved that semiconducting TiO<sub>2</sub> is an excellent photocatalyst to remedy energy sources and environment because of its strong oxidizing power, non-toxicity, and it can eliminate effectively pollutants in atmosphere and water [4–7]. However, it requires ultraviolet (UV) radiation whose energy exceeds the band gap

of 3.2 eV ( $\lambda \approx 380$  nm) of the anatase crystalline phase, hence, practically showing photocatalytic activity only under UV-light irradiation that accounts for only a small fraction of the solar energy. Many research groups proposed that the absorption edge of TiO<sub>2</sub> had been extended to the visible-light region by doping with transition metals and/or non-metals [8–14]. Nevertheless, only a slight shift to the visible light region can be resulted from the low content of the dopant species and thermal instability was posed with increasing the content of these dopant species [11,12]. Some photocatalysts are capable of extending the absorption edge to visible light, they do not warrant enhances visible light photocatalytic activity in a certain region of solar light [13,14]. Therefore, it is highly desirable for the design and construction of effective photocatalyst with strong absorption, high thermal stability, and facilitating the separation and transfer of the photogenerated carriers to develop efficient photocatalysts.

\* Corresponding author. Tel.: +86 37123889990.

\*\* Corresponding author.

E-mail addresses: wangyx@henu.edu.cn (Y. Wang), yangjianjun@henu.edu.cn (J. Yang).

More recently, a novel anatase  $\text{TiO}_2$ , containing a large amount of the intrinsic defects: single-electron-trapped oxygen vacancy (SETOV, denoted as  $\text{V}_0^\bullet$ ), was obtained by our group via heating nanotubular titanic acid (NTA) under high temperature conditions. Although the novel  $\text{V}_0^\bullet\text{-TiO}_2$  not only extends distinctly photo-response to visible-light region but also has excellent stability, this novel  $\text{TiO}_2$  has not any photocatalytic activity under visible light irradiation [15–17]. However, compared with the corresponding sample obtained using P25 as Ti source under the same condition,  $\text{V}_0^\bullet\text{-TiO}_2$  possessing high photocatalytic activity and excellent stability can be achieved upon doping or modifying NTA using other elements and/or compounds, such as Pt, N, Ag, and  $\text{AgCO}_3$  [18–25]. Vanadium ions doped  $\text{TiO}_2$  has been one of the frequent topics of the investigation, because it can apparently extend the light absorption of  $\text{TiO}_2$  into visible light region and increases carrier lifetime [8,26–32]. It seems one of the best alternatives to improve visible light absorption and photocatalytic activity under visible light illumination by the doping NTA using vanadium, which is attributed to the following reasons: (i) V ions with different valence state ( $\text{V}^{3+}\text{-}\text{V}^{5+}$ ), which contains the ability to transfer among  $\text{V}^{3+}\text{-}\text{V}^{5+}$  under reducing and oxidizing conditions. For example,  $\text{V}^{4+}$  ions can be easily formed through the reduction of  $\text{V}^{5+}$  trapping one electron from  $\text{V}_0^\bullet$  when NTA was dehydrated at different temperature in air. (ii)  $\text{V}^{4+}$  ions are easier to substituting for  $\text{Ti}^{4+}$  in the  $\text{TiO}_2$  crystal lattice because that the ion radii of  $\text{V}^{4+}$  (0.72 Å) compared with  $\text{V}^{5+}$  (0.68 Å) is much closer to that of  $\text{Ti}^{4+}$  (0.74 Å) and the tetragonal crystal structure of  $\text{VO}_2$  is similar to that of  $\text{TiO}_2$ , which is responsible for increased visible light absorption and photogenerated electrons ( $e^-$ ) and holes ( $h^+$ ) [33–44]. (iii) The photogenerated  $e^-$  and  $h^+$  can be trapped, be migrated to and be released in the surface of  $\text{TiO}_2$  by  $\text{V}^{4+}$  ions, which play a role of charge transfer species.  $\text{V}^{5+}$  ions were difficult to enter the lattice of  $\text{TiO}_2$ , which were apt to form  $\text{V}_2\text{O}_5$  in the surface and were responsible for  $e^-$  and  $h^+$  separation [35,36,41–44]. Subsequently, these photogenerated  $e^-$  and  $h^+$  can be accepted by the adsorbed  $\text{O}_2$  and surface hydroxyl group ( $\text{OH}^-$ ), and then transform  $\text{O}_2$  and  $\text{OH}^-$  into superoxide radicals ( $\bullet\text{O}_2^-$ ) and hydroxyl radical ( $\bullet\text{OH}$ ) active species, respectively.

Motivated by the previous successful applications of the doping or modifying NTA, the current work focuses on the design and synthesized V-doped  $\text{TiO}_2$  ( $\text{V-TiO}_2\text{[NTA]}$ ) photocatalyst using NTA as  $\text{TiO}_2$  precursor. Firstly, we calculated the formation energies ( $E_{\text{form}}$ ) of  $\text{V}_0^\bullet$ -doped  $\text{TiO}_2$  ( $\text{V}_0^\bullet\text{-TiO}_2$ ),  $\text{V}+\text{V}_0^\bullet$  co-doped  $\text{TiO}_2$  ( $\text{V}+\text{V}_0^\bullet\text{-TiO}_2$ ) and  $\text{V}+\text{V}_0^{2+}$  co-doped  $\text{TiO}_2$  ( $\text{V}+\text{V}_0^{2+}\text{-TiO}_2$ ) based on the density function theory (DFT) calculation. The results show that  $\text{V}+\text{V}_0^{2+}\text{-TiO}_2$  is more-favorable energetically. Secondly, we synthesized  $\text{V-TiO}_2\text{[NTA]}$  photocatalyst using NTA as  $\text{TiO}_2$  precursor and the photocatalytic activities of as-achieved  $\text{V-TiO}_2\text{[NTA]}$  samples in visible light region were quantitatively evaluated by monitoring photocatalytic oxidation of propylene ( $\text{C}_3\text{H}_6$ ). Propylene is one of the most important chemicals. When it is used to synthesize other compounds, it may spread into air, which will endanger people's health and will produce an inflammable and explosive gas mixture. Therefore, it is valuable to explore the degradation of propylene by catalysis. In addition, the degradation products of  $\text{C}_3\text{H}_6$  are very simple (only  $\text{CO}_2 + \text{H}_2\text{O}$ ), which is beneficial for evaluating the photocatalytic efficiency of V-doped  $\text{TiO}_2$ . The result reveals that the photocatalytic activity of  $\text{V-TiO}_2\text{[NTA]}$  catalysts for the removal of  $\text{C}_3\text{H}_6$  under visible light irradiation is significantly better than that of the as-prepared NTA, P25  $\text{TiO}_2$ , N- $\text{TiO}_2\text{[NTA]}$ , and V-doped P25- $\text{TiO}_2$  ( $\text{V-P25-TiO}_2$ ). Finally, through a series of characterization techniques including Raman spectra, TEM, XPS and UV-vis and electronic structures, we propose a new  $\text{V}^{4+}$  ions formation mechanism by means of the electron trapped at SETOV not  $\text{Ti}^{3+}$  [43,44]. The incorporation of  $\text{V}^{4+}$  in  $\text{TiO}_2$  bulk lattice induces some new hybrid states near the edge of the valence and conduction bands, respectively, causing an effective narrowing of the band gap. The

narrowing of gap is responsible for the red-shifted and increased light-absorption. The presence of surface  $\text{V}^{5+}$ /bulk  $\text{V}^{4+}$  redox couple facilitates the efficient separation and migration of photogenerated  $e^-/h^+$  pairs to generate active species. These finding establish the synergistic effect between bulk doping and surface doping for enhanced photocatalytic activity as a powerful guiding principle in the future design of photocatalysts and other functional materials.

## 2. Experimental methods and computational details

### 2.1. Synthesis of nanotube titanic acid ( $\text{H}_2\text{Ti}_2\text{O}_4(\text{OH})_2$ , NTA)

The preparation procedure of NTA was described as follows: an appropriate amount of Degussa P25- $\text{TiO}_2$  powder was added into certain concentrations of NaOH aqueous solution (10 mol/L) under continuous stirring for 30 min to achieve uniform dispersion. The resultant mixture was transferred into an autoclave to carry out hydrothermal reaction at 120 °C for 24 h. After cooling to room temperature, removing the supernatant, the obtained white precipitate was washed deionized water repeatedly to a pH of ca. 7–8, and then dipped with HCl solution (0.1 mol/L) for 7 h under magnetic stirring for performing enough ion exchange between  $\text{Na}^+$  and  $\text{H}^+$ . Subsequently, as-achieved precipitate was washed again with deionized water many times to remove  $\text{Cl}^-$  and at room temperature under vacuum. The resultant product was NTA.

### 2.2. Preparation of V-doped $\text{TiO}_2$ ( $\text{V}_0^\bullet$ )

An amount of 1 g the above prepared NTA powder was added into 15 mL of aqueous solution of hydrogen peroxide (2 wt%) and then known amounts of ammonia metavanadate solution ( $\text{NH}_4\text{VO}_3$ , 0.01 mol/L), acting as the source of V, added dropwise into NTA suspension (with molar ratios of  $\text{V}/\text{Ti} = 0\%, 0.1\%, 0.3\%, 0.5\%, 1\%, 2\%, 5\%$ , and 10%) under continuous stirring. The obtained mixture was stirred at 40 °C for 4 h to allow uniform disperse, followed by vacuum distillation at 50 °C. The obtained uniform mixture of solid phase was dried overnight at 80 °C under vacuum and then further heated in air at 400 °C for 4 h to form  $\text{V-TiO}_2$  ( $\text{V}_0^\bullet$ ) with different V doping content denoted as  $x\%\text{-TiO}_2\text{[NTA]}$  (400). The sample of the different heat treatment temperature with 1% V doping level was also prepared by annealing at 300, 500, 600, 700, and 800 °C in air for 4 h, respectively, to further investigate the effect of calcination temperatures on the physical and chemical properties of the as-prepared catalysts and the obtained photocatalysts were denoted as 1% $\text{-TiO}_2\text{[NTA]}$  (300–800).

### 2.3. Structural characterization of catalysts

Powder XRD patterns for as-obtained photocatalysts were recorded with a Bruker D8 advance diffractometer. A transmission electron microscope (TEM), JEOL JEM-2010 with accelerating voltage 200 kV, was applied to observe the morphology of catalysts. All UV-vis diffuse reflectance spectroscopic (DRS) experiments were carried out on a Shimadzu U-4100 spectrometer and a CARY5000 spectrometer using  $\text{BaSO}_4$  as a standard. The catalysts of X-ray photoelectron spectroscopy data were obtained through a Kratos AXIS Ultra spectrometer using monochromatized  $\text{Al-K}\alpha$  ( $h\nu = 1486.6$  eV) radiation as excitation source. The binding energies were referenced to C 1s line at 284.8 eV from adventitious carbon. The Brunauer–Emmett–Teller (BET) specific surface area of the samples were determined by using nitrogen adsorption with surface area analyzer (Quadasorb SI-4). Electron spin resonance (ESR) spectra were recorded on a Bruker E500 spectrometer at room temperature in ambient air (without supplied vacuum).

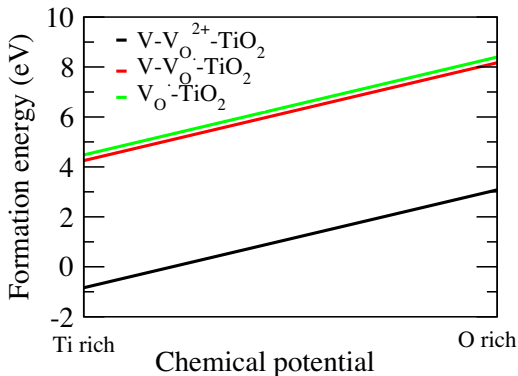


**Fig. 1.** Calculated formation energy for the  $V_o^{\bullet}-TiO_2$ ,  $V+V_o^{\bullet}-TiO_2$ , and  $V+V_o^{2+}-TiO_2$  as a function of the chemical potential of Ti and O.

#### 2.4. Computational details

The geometry structural optimization and electronic structure calculations were performed to the defect-free anatase  $TiO_2$ ,  $V_o^{\bullet}$  (i.e., SETOV, a singly ionized oxygen vacancy with +1 charge)- $TiO_2$ , V-doped  $TiO_2$  ( $V-TiO_2$ ), and  $V+V_o^{2+}$  (a doubly ionized oxygen vacancy, with +2 charge)- $TiO_2$ . The calculations were performed within the spin polarized density functional theory (DFT) using the Vienna ab initio simulation package (VASP) [45,46]. The general gradient approximation (GGA) [47] in the scheme of Perdew–Burke–Ernzerhof (PBE) [48] was chosen to describe the exchange and correlation potential, and the projector augmented wave method (PAW) [49] was used for the core–valence interactions. The electronic structures of the corresponding optimized geometries was calculated by GGA+U method. To reach an agreement with the experimental band gap of anatase  $TiO_2$ , the  $U$  parameter ( $U_{eff} = 5.8$  eV [50] for the Ti 3d orbit and  $U_{eff} = 7.0$  eV [51] for the V 3d orbit) was used. A  $2 \times 2 \times 2$  supercell containing 32 Ti atoms and 64 O atoms was simulated for anatase  $TiO_2$ . The V-doped anatase  $TiO_2$  was modeled by replacing one titanium atom with V in the 96 atoms anatase supercell. A  $V_o^{\bullet}$  and  $V_o^{2+}$  states were created by removing one oxygen atom from  $TiO_2$  and V-doped  $TiO_2$  models. We used a kinetic energy cutoff of 500 eV to obtain more accurate results. Several  $k$ -point sampling were performed for convergence tests, and the Brillouin zone  $k$ -mesh of  $3 \times 3 \times 1$  was used for geometry optimization and electronic property calculations, which was found to be sufficient to reach convergence for the supercells. To find the most stable lattice structure, both atomic positions and lattice parameters were relaxed. When the forces on each atom was less than 0.02 eV/Å and the total energy change was less than  $10^{-7}$  eV, the iterative process was considered to be convergence.

#### 2.5. Evaluation of photocatalytic activity

The photocatalytic activities of as-prepared catalysts were evaluated by the photocatalytic oxidation of gaseous  $C_3H_6$  under visible light irradiation. A 300 W Xe lamp equipped with a  $\lambda = 420$  nm glass filters to remove UV light was used as a source of visible light. A flat quartz tube was used as the photocatalysis reactor. To carry out photocatalytic tests, 30 mg photocatalyst powder was first dispersed in a small amount of deionized water and stirred evenly. And then the obtained suspension was evenly spread on one side of a roughened glass plate (ca.  $7.8\text{ cm}^2$ ) that was mounted in the middle of the quartz tube reactor. A water cell was also inserted between the xenon lamp and reactor to eliminate infrared light and the distance between them is about 7 cm. The gas mixture of propylene and air stored in a high-pressure cylinder was used as feed gas, and the flow rate of the gas was fixed to ca. 150 mL/h. The

concentration of  $C_3H_6$  was determined using a chromatograph (Shimadzu GC-9A) equipped with a flame ionization detector (FID), a GDX-502 column, and a reactor loaded with Ni catalyst for the methanization of  $CO_2$ . Prior to light irradiation, the coated glass plate was kept in the dark for ca. 2 h to achieve the absorption/desorption equilibrium of  $C_3H_6$  on the photocatalyst surfaces. The photo-oxidation removal rate of  $C_3H_6$  over various photocatalysts was calculated as  $(C_0 - C)/C_0 \times 100\%$ , where  $C_0$  refers to the initial concentration of feed gas  $C_3H_6$  (600 ppmv,  $\sim 12\text{ }\mu\text{mol}$ ) and  $C$  refers to the concentration of  $C_3H_6$  measured upon the completion of its photocatalyzed oxidation.

### 3. Results and discussion

#### 3.1. Formation Energy

In thermodynamic equilibrium, the formation energy ( $E_{q,\alpha}^f$ ) of defect  $\alpha$  with a charge  $q$  in  $TiO_2$  is given by expression [52]  $E_{q,\alpha}^f = E_{q,\alpha} - E_{TiO_2} + n_\alpha \mu_\alpha + q(E_F + E_V + \Delta V)$ , where  $E_{q,\alpha}^f$  is the total energy of supercell containing the defect  $\alpha$  in charge state  $q$ ,  $E_{TiO_2}$  is the total energy of a  $TiO_2$  perfect crystal in the same supercell,  $\mu_\alpha$  is the chemical potential of  $\alpha$  element,  $n_\alpha$  is the number of atoms removed during the defect formation from the host crystal, and its sign is positive and vice versa.  $E_F$  is the Fermi energy and  $E_V$  is the valence-band maximum of the host crystal.  $\Delta V$  aligns the reference potential in one defect supercell with that in the bulk. For  $V_o^{\bullet}-TiO_2$ ,  $V+V_o^{\bullet}-TiO_2$ , and  $V+V_o^{2+}-TiO_2$  systems, their formation energies ( $E_{V_o^{\bullet}-TiO_2}^f$ ,  $E_{V+V_o^{\bullet}-TiO_2}^f$ , and  $E_{V+V_o^{2+}-TiO_2}^f$ ) were calculated by following Eqs. (1)–(3), respectively:

$$E_{V_o^{\bullet}-TiO_2}^f = E_{V^{\bullet}-TiO_2} - E_{TiO_2} + \mu_{Ti} + (E_F + E_{Ti} + \Delta V) \quad (1)$$

$$E_{V+V_o^{\bullet}-TiO_2}^f = E_{V+V_o^{\bullet}-TiO_2} - E_{V-TiO_2} + \mu_O + (E_F + E_V + \Delta V) \quad (2)$$

$$E_{V+V_o^{2+}-TiO_2}^f = E_{V+V_o^{2+}-TiO_2} - E_{V-TiO_2} + \mu_O + 2(E_F + E_V + \Delta V) \quad (3)$$

where  $E_{TiO_2}$ ,  $E_{V_o^{\bullet}-TiO_2}$ ,  $E_{V+V_o^{\bullet}-TiO_2}$ , and  $E_{V+V_o^{2+}-TiO_2}$  are the total energies of  $TiO_2$ ,  $V_o^{\bullet}-TiO_2$ ,  $V+V_o^{\bullet}-TiO_2$ , and  $V+V_o^{2+}-TiO_2$  systems. The  $\mu_{Ti}$  and  $\mu_O$  are the chemical potentials of Ti and O. The formation energy depends on growth conditions, which may be varied from Ti- to O-rich. Limited by the thermodynamic stability condition for  $TiO_2$ , Ti and O are variables correlated as  $2\mu_O + \mu_{Ti} = \mu(TiO_2) = \mu_{Ti[bulk]} + 2\mu_{O[O_2]} + \Delta H(TiO_2)$ , where  $\Delta H(TiO_2)$  is the enthalpy of formation of bulk  $TiO_2$ . The calculated formation enthalpy of  $TiO_2$  is  $-10.25$  eV, which is close to the previous result  $-10.3$  eV [53]. Thus, under the O-rich limit condition,  $\mu_O = \frac{1}{2}E_O$ ,  $\mu_{Ti} = \Delta H(TiO_2) + \mu_{Ti[bulk]}$ ; similarly, under the Ti-rich limit condition,  $\mu_{Ti} = \mu_{Ti[bulk]} = E_{Ti[bulk]}$ ,  $\mu_O = \frac{1}{2}[\Delta H(TiO_2) + \mu_{O[O_2]}]$ .

Fig. 1 shows the calculated defect formation energy of the  $V_o^{\bullet}-TiO_2$ ,  $V+V_o^{\bullet}-TiO_2$ , and  $V+V_o^{2+}-TiO_2$  systems. The calculated formation energies for the  $V_o^{\bullet}-TiO_2$  and  $V_o^{2+}-TiO_2$  in the presence of V doping are 4.27 and  $-0.84$  eV under Ti-rich, respectively. Under O-rich conditions, the values are 8.19 and 3.08 eV, respectively. From this, we can see that it is energetically more favorable to form the  $V+V_o^{\bullet}-TiO_2$  and  $V+V_o^{2+}-TiO_2$  systems than to form the  $V_o^{\bullet}$ -monodoped  $TiO_2$  (4.48 and 8.40 eV) whether in the conditions of Ti-rich or O-rich. This suggests that the  $V+V_o^{\bullet}$  co-doping is relatively more facilitated than  $V_o^{\bullet}$  monodoping by the electrostatic attraction of the two dopants with opposite charge states. A similar phenomenon is also reported in Ref. [53]. From Fig. 1, we can see that the  $V+V_o^{2+}-TiO_2$  systems is most-favorable energetically.

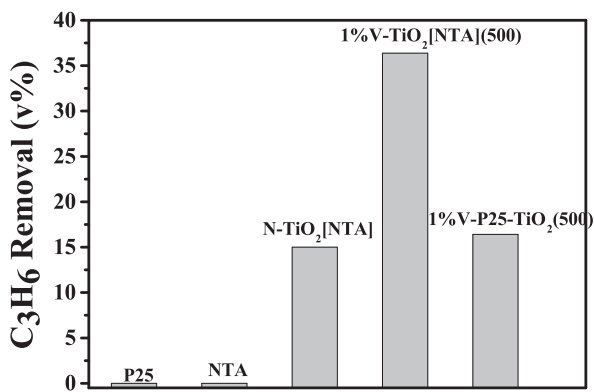


**Fig. 2.** Comparison of the visible light photocatalytic activity of P25-TiO<sub>2</sub>, as-prepared NTA, N-TiO<sub>2</sub>[NTA], 1%V-TiO<sub>2</sub>[NTA] (500), and 1%V-P25-TiO<sub>2</sub>(500) for photocatalytic oxidation of propylene.

### 3.2. Comparison tests of photocatalytic activity

To demonstrate the remarkable photocatalytic activity of synthesized V-TiO<sub>2</sub>[NTA] samples, we compare its photocatalytic

performance with as-prepared NTA, P25-TiO<sub>2</sub>, N-TiO<sub>2</sub>[NTA], and V-P25-TiO<sub>2</sub>, as shown in Fig. 2. It can be seen that P25-TiO<sub>2</sub> and as-prepared NTA have no any photoactivity (almost zero) for photocatalytic degradation of propylene. When a small amount of V (1%) is doped into TiO<sub>2</sub>, the photocatalytic activity of the obtained sample 1%V-TiO<sub>2</sub>[NTA] (500) increases significantly, which is 2 times higher than that of the N-TiO<sub>2</sub>[NTA] [34] and V-P25-TiO<sub>2</sub>.

### 3.3. X-ray diffraction (XRD) patterns and Raman spectra of the photocatalysts

Fig. 3 shows X-ray diffraction patterns of V-TiO<sub>2</sub>[NTA] samples with different V doping content annealed at 400 °C and 1%V-TiO<sub>2</sub>[NTA] (300–700 °C), where the inset is XRD pattern of as-prepared NTA. The as-prepared NTA has a diffraction peak at  $2\theta = 8.6^\circ$ , which is the characteristic peak of tubular structure of NTA. NTA belongs to orthorhombic system in terms of crystal structure, which has been well elucidated elsewhere [15–25]. The effects of V doping concentration on the phase structures of the TiO<sub>2</sub> powders are shown in Fig. 3a. All samples exhibit only anatase patterns at annealing temperature of 400 °C. The intensity of diffraction peak of TiO<sub>2</sub> (101) plane gradually became weaker as the V

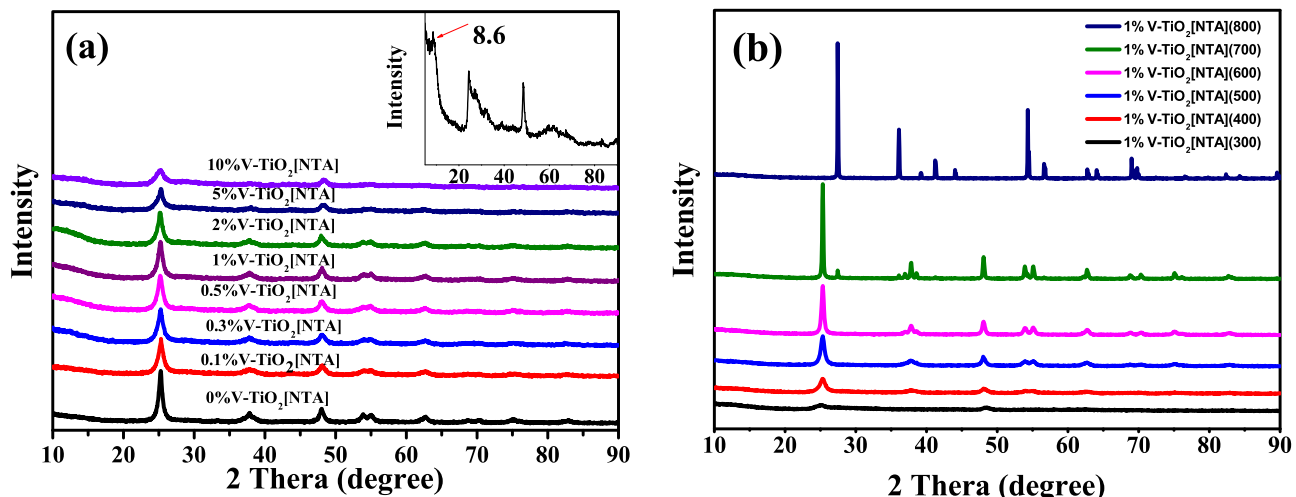


**Fig. 3.** X-ray diffraction patterns of (a) x%V-TiO<sub>2</sub>[NTA] (400) series of samples, (b) 1%V-TiO<sub>2</sub>[NTA] (annealed at 300–800 °C). The inset in (a) is as-prepared NTA.

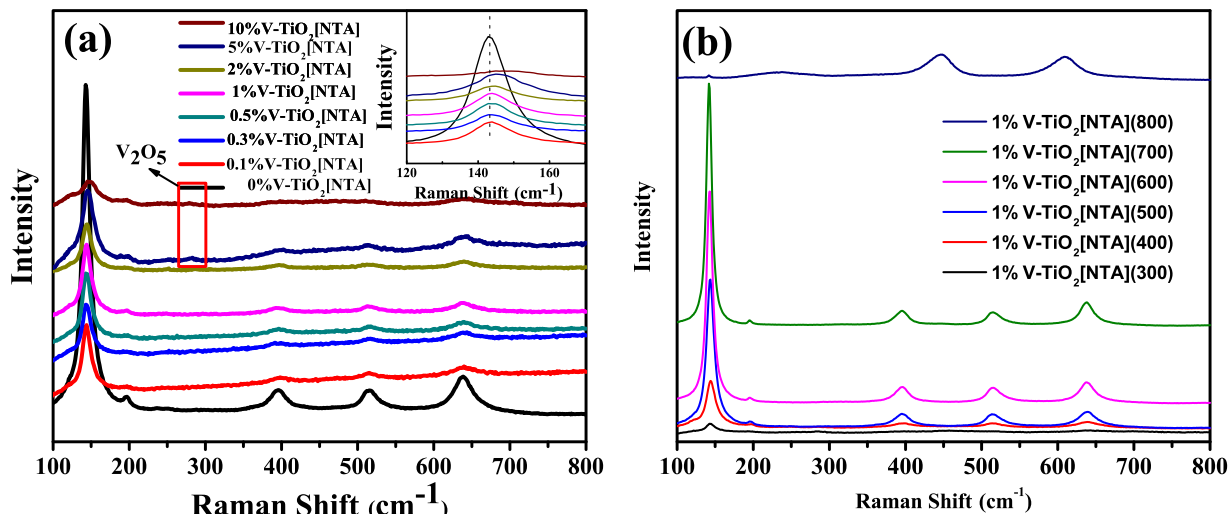


**Fig. 4.** Raman spectra of (a) x%V-TiO<sub>2</sub>[NTA] (400) series of samples, (b) 1%V-TiO<sub>2</sub>[NTA] (annealed at 300–800 °C). The inset of (a) is magnified Raman pattern from 120 to 170 cm<sup>-1</sup> of x%V-TiO<sub>2</sub>[NTA] (400).

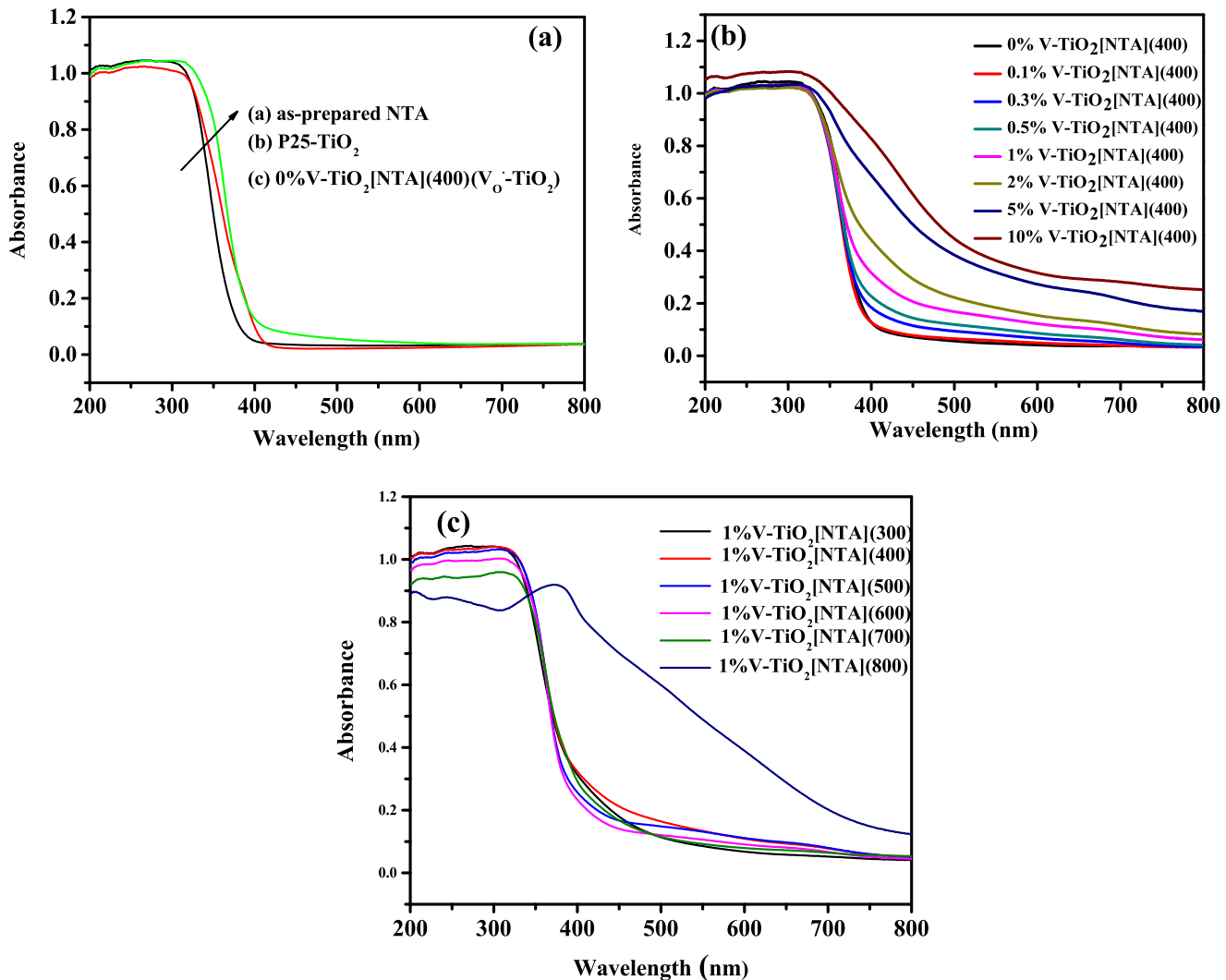


**Fig. 5.** UV-vis absorption spectra of (a) as-prepared NTA, P25-TiO<sub>2</sub> and 0%V-TiO<sub>2</sub>[NTA] (400), (b) V-TiO<sub>2</sub>[NTA] series of samples (annealed at 400 °C), and (c) 1%V-TiO<sub>2</sub>[NTA] (annealed at 300–800 °C).

concentration increased. It indicates that the larger the amount of V doping is, the poorer the crystallization of the TiO<sub>2</sub> powders is, and the smaller the crystallite size of TiO<sub>2</sub> is. No obvious diffraction peaks corresponding to vanadium oxides (such as V<sub>2</sub>O<sub>5</sub> and/or VO<sub>2</sub>) were observed according to XRD pattern, indicating that either V is incorporated into the crystal lattice of TiO<sub>2</sub> or vanadium oxide is very small and homogeneously dispersed. However, V doping concentration increasing to 5%, the obvious decrease of the peak intensity of anatase can be observed, which might be related to the existence of surface V<sub>2</sub>O<sub>5</sub>. The amount and the crystallites size of V<sub>2</sub>O<sub>5</sub> or VO<sub>2</sub> were too low and little to be detected by XRD technique, as well as these oxides were yet not detected by XRD for their high dispersion in the sample, but it can be seen additional peaks corresponding to V<sub>2</sub>O<sub>5</sub> in the high V doping concentration [36,42,54] by means of Raman technique. It is well known that Raman spectroscopy can detect even minor amount of material phase. To further determine whether the vanadium oxides exist, we analyze Raman spectra of samples with different V doping content, as shown in Fig. 4. Indeed, when the concentration of V doping increases to 5%, it begins to produce additional Raman peaks corresponding to V<sub>2</sub>O<sub>5</sub> phase (Fig. 4a). The inset in Fig. 4a is the magnified Raman patterns from 120 to 170 cm<sup>-1</sup>. It can be seen that (101) plane diffraction peak slightly shifts toward the right. The shift of the diffraction peak

may be ascribed to the fact that V<sup>4+</sup> ions are doped into TiO<sub>2</sub> lattice, substituting for Ti<sup>4+</sup> ions, and forming the V—O—Ti bond because the ion radius of V<sup>4+</sup> (0.72 Å) and Ti<sup>4+</sup> (0.74 Å) are very close [34–37]. At the same time, the rutile phase is not observed, even in the case of 10% V doping level, which indicates that using NTA as the titanium source to synthesize V-TiO<sub>2</sub>[NTA] may preserve the stability of anatase phase to some extent.

Figs. 3b and 4b show XRD and Raman pattern of the samples with 1% V modification level calcined at different temperatures, respectively. It can be seen that the calcination temperatures have an obviously influence on the crystallization of the sample. At  $T \leq 600$  °C, 1%V-TiO<sub>2</sub>[NTA] samples only possess pure anatase phase of TiO<sub>2</sub>. The sample calcined at 700 °C shows a mixcrystal structure with anatase as the major phase and rutile as the minor phase. Whereas the sample calcined at 800 °C is opposite, rutile TiO<sub>2</sub> as the major phase exists. Depending on the method of preparation, titanium precursor, and the presence of suitable dopant oxides, titania can undergo a phase transformation from the low-temperature anatase phase to rutile above 450 °C and is seen to extend to as high as 1000 °C [55]. Yang et al. reported that doping vanadium oxide within TiO<sub>2</sub> would have a stabilizing effect on the Ti—O bond because the more electropositive V<sup>4+</sup> and/or V<sup>5+</sup> will render its electronic concentration to O<sup>2-</sup> so that it can use this increased concentration of electrons to strengthen the bonding between the

less electropositive  $Ti^{4+}$  ions [35]. This stabilization of  $Ti-O$  bond will in turn retard the anatase–rutile transformation temperature because the anatase–rutile transformation needs the breakage of  $Ti-O$  bonds. To further demonstrate the effect of annealing temperature on the formation of  $V_2O_5$  and/or  $VO_2$ , the samples with 1% V modification level calcined at different temperatures were also given Raman spectra measurement, as illustrated in Fig. 4b. In the range 300–700 °C of annealing temperature, no obvious peaks corresponding to  $V_2O_5$  and/or  $VO_2$  are detected, indicating that annealing temperature has no effect on the formation of vanadium oxide. Of course, this may also be related to the low concentration of V doping (1 mol%).

### 3.4. UV-vis diffuse reflectance spectra (UV-vis DRS)

The UV-vis optical absorption spectra obtained by the diffuse reflectance of as-prepared NTA, P25-TiO<sub>2</sub> and  $V_o^{\bullet\bullet}$ -TiO<sub>2</sub> (0%V-TiO<sub>2</sub>[NTA] (400)) are presented in Fig. 5a. As-prepared orthorhombic system NTA and the commercially available P25-TiO<sub>2</sub>, with white color, show absorption thresholds at ~380 and ~410 nm corresponding to the interband transition, and indicating band gaps of 3.26 and 3.0 eV, respectively. Compared with NTA, the absorption of P25-TiO<sub>2</sub> extends to a longer wavelength region to some extent, which may be owing to a large band gap of NTA than that of P25-TiO<sub>2</sub> (a mixture of anatase phase ( $E_g$  of 3.2 eV) and rutile phase (3.0 eV)). In contrast, the achieved  $V_o^{\bullet\bullet}$ -TiO<sub>2</sub> using the same preparation method as V-doped TiO<sub>2</sub> without adding NH<sub>4</sub>VO<sub>3</sub>, exhibits obvious visible-light absorption property compared with NTA and P25, though possessing the same white color, which originates from the generation of a large amount of  $V_o^{\bullet\bullet}$  [15,20,22]. As for V-TiO<sub>2</sub>[NTA] catalysts, it is apparent that the DRS of all the doped TiO<sub>2</sub> samples have extended a red shift and increased absorbance in the visible range with increasing doping content, in accordance with the observed color change of the samples from faint yellow to dark brown with increasing V concentrations. The absorption edge shift of V-doped TiO<sub>2</sub> has been reported in many literatures [35,38,41,56,57], in which the  $V^{4+}$  was considered to be chiefly responsible for the visible light absorption. The presence of a large amount of paramagnetic oxygen vacancy can extend absorption of TiO<sub>2</sub> in the visible light region, as above mentioned. A red shift and increased absorbance in the visible range with increasing doping content can be explained by many  $V^{4+}$  substituting  $Ti^{4+}$  at higher doping content. When annealing temperature was performed in the range of 300–700 °C, no significant change was observed in the absorption of 1%V-TiO<sub>2</sub>[NTA] samples in the visible light region. However, as annealing temperature was raised to 800 °C, a broad and strong visible-light band almost covering the whole visible region and even near-infrared region. An analysis of XRD and Raman spectra shows that the observed broad and strong absorption may be related to more defect states (such as: sepias) and the existence of  $V_2O_5$  (such as its band gap: 2.14 eV) at 800 °C.

**Table 1**

The specific surface area ( $S_{BET}$ ) of as-prepared NTA and x%V-TiO<sub>2</sub>(400).

Samples $S_{BET}$	as-prepared NTA	0%V-TiO <sub>2</sub> [NTA] (400)	0.5%V-TiO <sub>2</sub> [NTA] (400)	1%V-TiO <sub>2</sub> [NTA] (400)	2%V-TiO <sub>2</sub> [NTA] (400)	5%V-TiO <sub>2</sub> [NTA] (400)
$S_{BET}$ (m <sup>2</sup> /g)	390.64	139.254	226.518	227.911	237.571	300.079

**Table 2**

The specific surface area ( $S_{BET}$ ) of 1%V-TiO<sub>2</sub>(300–800 °C).

Samples $S_{BET}$	1%V-TiO <sub>2</sub> [NTA] (300)	1%V-TiO <sub>2</sub> [NTA] (400)	1%V-TiO <sub>2</sub> [NTA] (500)	1%V-TiO <sub>2</sub> [NTA] (600)	1%V-TiO <sub>2</sub> [NTA] (700)	1%V-TiO <sub>2</sub> [NTA] (800)
$S_{BET}$ (m <sup>2</sup> /g)	334.383	227.911	99.383	69.334	17.526	0.172

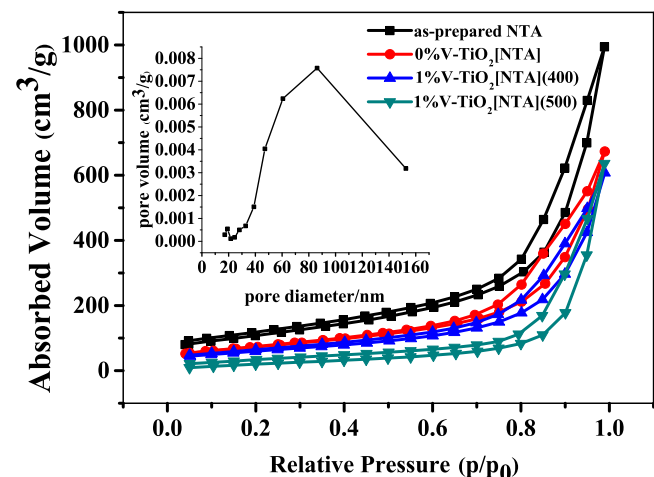


**Fig. 6.**  $N_2$  adsorption–desorption isotherms of as-prepared NTA, 0%V-TiO<sub>2</sub>[NTA] (400) and 1%V-TiO<sub>2</sub>[NTA] (500). The inset is pore size distributions curve of the sample 1%V-TiO<sub>2</sub>[NTA] (500).

### 3.5. BET surface areas and pore distributions

The changes in surface area ( $S_{BET}$ ) and pore size distribution of the V-TiO<sub>2</sub>[NTA] were examined. Fig. 6 shows the adsorption–desorption isotherms of as-prepared NTA, 0%V-TiO<sub>2</sub>[NTA] (400), 1%V-TiO<sub>2</sub>[NTA] (400), and 1%V-TiO<sub>2</sub>[NTA] (500), as well as the pore size distributions curve (inset) of the sample 1%V-TiO<sub>2</sub>[NTA] (500). All of the samples exhibited similar type-IV isotherms with an H3 hysteresis loop at high relative pressure range of 0.50–0.99, which are typical characters of mesoporous materials [58]. The  $S_{BET}$  of the as-prepared NTA, x%V-TiO<sub>2</sub>[NTA] (400), and the 1%V-TiO<sub>2</sub>[NTA] (300–800) are summarized in Tables 1 and 2, respectively. The  $S_{BET}$  of the three samples as-prepared NTA, 0%V-TiO<sub>2</sub>[NTA] (400), and 1%V-TiO<sub>2</sub>[NTA] (400) are 390.64, 139.254, and 227.911 m<sup>2</sup>/g, respectively. We also find that the  $S_{BET}$  of x%V-TiO<sub>2</sub>[NTA] (400) increases with increasing V concentrations, because vanadium species implantation inhibited crystalline growth, thereby enlarging the surface area, which is conformance with the change observed of the diffraction peak, as above mentioned. The increase of  $S_{BET}$  can improve the activity of catalyst. The  $S_{BET}$  of the 1%V-TiO<sub>2</sub>[NTA] (400) and 1%V-TiO<sub>2</sub>[NTA] (500) decreased from 217.911 to 99.383 m<sup>2</sup>/g, with the increasing of calcination temperature, which can be attributed to the extent of crystallization increasing with the annealing temperature. From the inset, it can be seen that the diameter ranges of pores ( $d_p$ ) locate from 1.5 to 15.5 nm, the main concentration of these particles is at 9.0 nm. The formation of mesoporous structure in the powders is attributed to the aggregation of TiO<sub>2</sub> crystallites.

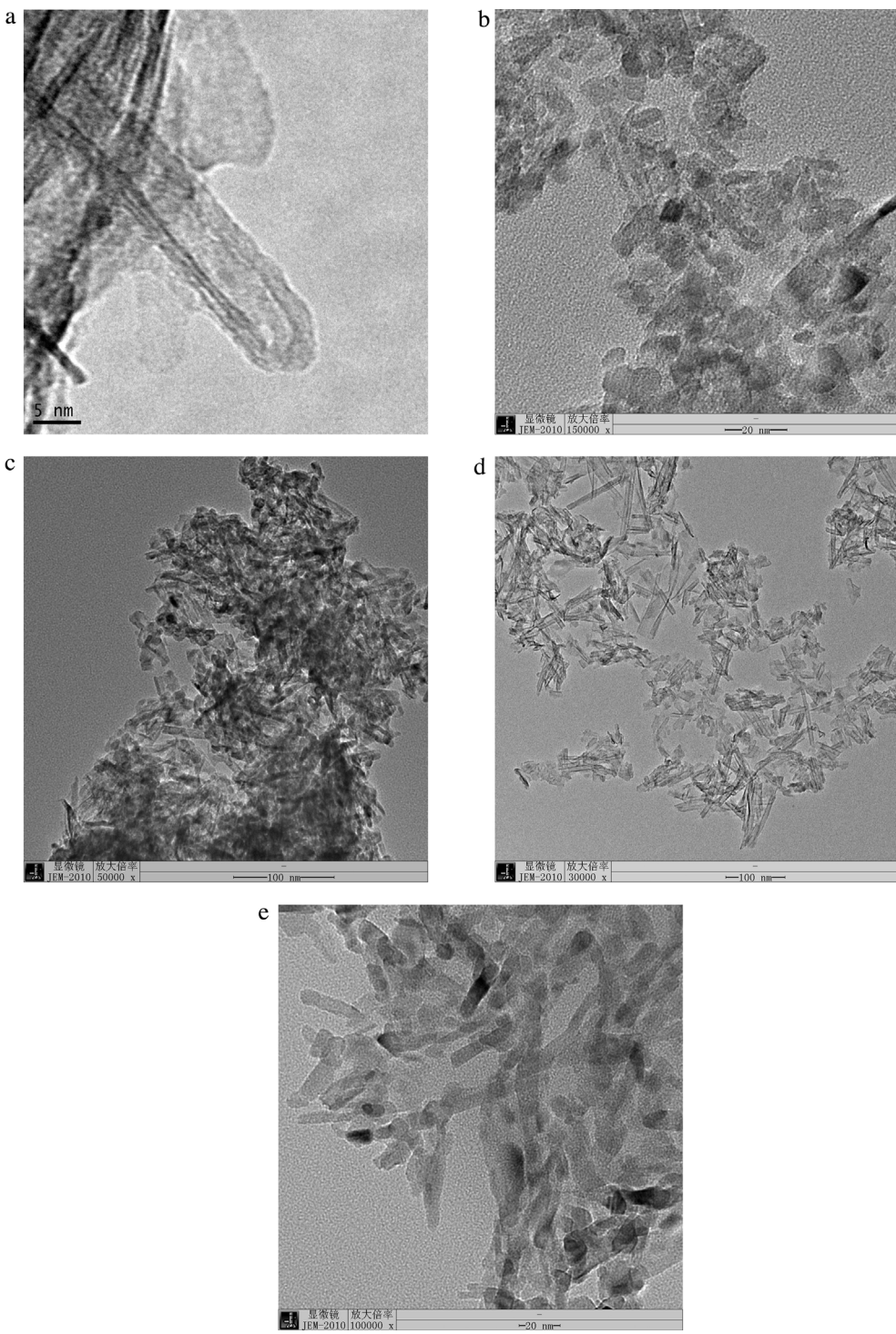


**Fig. 7.** TEM images of (a) as-prepared NTA, (b) 0%V-TiO<sub>2</sub>[NTA] (400), (c) 1%V-TiO<sub>2</sub>[NTA] (400), (d) 5%V-TiO<sub>2</sub>[NTA] (400), and (e) 1%V-TiO<sub>2</sub>[NTA] (500).

### 3.6. Morphology of catalysts

**Fig. 7** shows the results of TEM images of as-prepared NTA, 0%V-TiO<sub>2</sub>[NTA] (400), 1%V-TiO<sub>2</sub>[NTA] (400), 5%V-TiO<sub>2</sub>[NTA] (400), and 1%V-TiO<sub>2</sub>[NTA] (500) samples. From **Fig. 7a**, we can see that as-prepared NTA belonging to orthorhombic system has a layered structure with the distance between the adjacent layers ca. 0.8 nm, in accordance with previous research [29]. When as-prepared NTA is annealed at 400 °C for 4 h in air, accompanied by the formation of anatase phase, its nanotube morphology is slightly destroyed

(**Fig. 7b**). Compared with undoped TiO<sub>2</sub>, it is obviously seen that nanotube structure of the sample 1%V-TiO<sub>2</sub>[NTA] (400) and 5%V-TiO<sub>2</sub>[NTA] (400) has been kept with nanotube structure, displaying the better nanotube structure with the larger the amount of V doping (**Fig. 7c and d**). The result reveals that the presence of V dopant is favorable to keeping the nanotube structure, which is in accordance with the increasing of its  $S_{BET}$ . When 1%V-TiO<sub>2</sub>[NTA] is annealed at 500 °C for 4 h in air, it is in the highly crystallized particles, which is in accordance with its small  $S_{BET}$ . However, the studies behind demonstrate the photocatalytic activity of 1%V-TiO<sub>2</sub>[NTA] (500) is

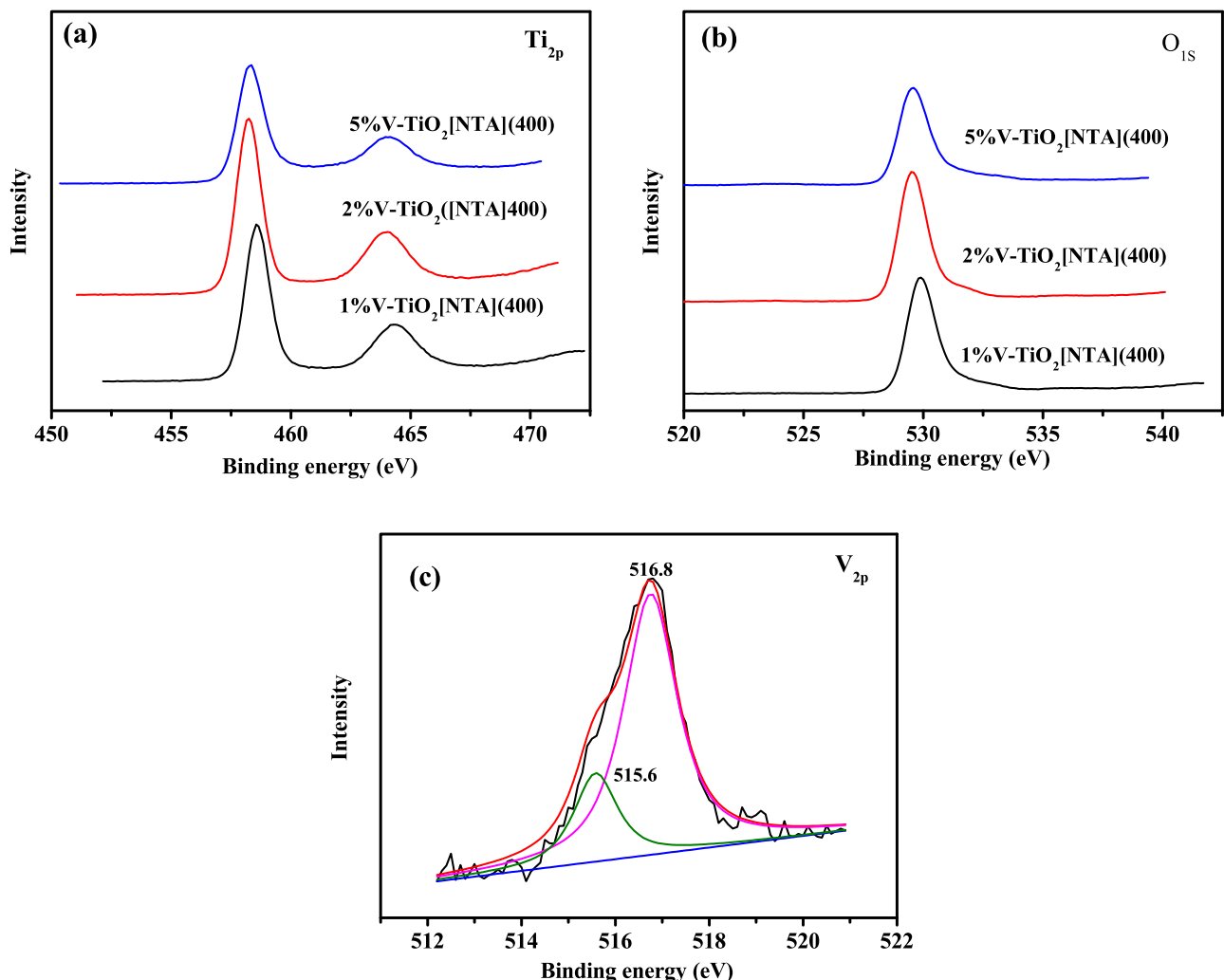


**Fig. 8.** XPS spectra of V-TiO<sub>2</sub>[NTA]: (a) Ti 2p, (b) O 1s, and (c) V 2p of 5%V-TiO<sub>2</sub>[NTA] (400).

the highest of all samples (see Section 3.10), which also indicates that  $S_{\text{BET}}$  is not the most important factor influencing the activity in this sample.

### 3.7. X-ray photoelectron spectroscopy (XPS)

The chemical compositions and states of surface elements in the modified TiO<sub>2</sub> were investigated by XPS analysis. The chemical states of Ti 2p, O 1s, and V 2p species were obtained by analyzing the XPS core levels (parts a–c of Fig. 8). As shown in (a) of Fig. 8, the binding energy of Ti 2p<sub>3/2</sub> shifted to a negative value by 0.20, 0.33, and 0.31 eV in 1%V-TiO<sub>2</sub>[NTA] (400), 2%V-TiO<sub>2</sub>[NTA] (400), and 5%V-TiO<sub>2</sub>[NTA] (400) compared with that of Ti 2p<sub>3/2</sub> (458.8 eV) in TiO<sub>2</sub> [59]. The lower binding energy of Ti 2p in V-TiO<sub>2</sub>[NTA] suggests the increased charge density of Ti due to the incorporation of vanadium into the lattice. Fig. 8(b) shows that the energy peak of O in V-TiO<sub>2</sub>[NTA] is all higher than that of O (529.9–530.2 eV) in pure TiO<sub>2</sub> (i.e., lattice oxygen), which could be due to the substitution of V ions for Ti ions leading to the decreased electron density of oxygen according to electronegativity of V element higher than that of Ti element. Based on the above analysis, it is further evident that the V ions are doped into TiO<sub>2</sub> lattice to substitute Ti<sup>4+</sup> ions, and form the V–O–Ti bond. The XPS spectrum of the V 2p region for 5%V-TiO<sub>2</sub>[NTA] (400) is shown in Fig. 8(c). The V species exist with a close binding energy value of V<sup>5+</sup> 2p<sub>3/2</sub> (516.4–517.4 eV) and V<sup>4+</sup> 2p<sub>3/2</sub> (515.4–515.7 eV) [35]. Therefore, the peak fitted at 516.8 eV can be

mainly ascribed to V<sup>5+</sup> 2p<sub>3/2</sub>, whereas that at 515.6 eV was assigned to V<sup>4+</sup> 2p<sub>3/2</sub>. The fitting data demonstrate that V<sup>5+</sup> was the dominant composition on the surface of doped TiO<sub>2</sub>. It has been reported that vanadium species (V<sup>5+</sup>) had the tendency to be on the surface [8]. Herein, we have detected the existence of V<sub>2</sub>O<sub>5</sub> via Raman spectra (see Section 3.1), which suggests that vanadium species (V<sup>5+</sup>) exist as the form of V<sub>2</sub>O<sub>5</sub> on the surface. While, the ionic radius of V<sup>4+</sup> is very close to that of Ti<sup>4+</sup>, and V<sup>4+</sup> can yet be easily substituted for the Ti<sup>4+</sup> into the TiO<sub>2</sub> crystal lattice [35,36,54,57].

### 3.8. Electron spin resonance (ESR) spectra

Fig. 9 illustrates the ESR spectra of as-prepared NTA, 0%V-TiO<sub>2</sub>[NTA] (400), 1%V-TiO<sub>2</sub>[NTA] (400), 2%V-TiO<sub>2</sub>[NTA] (400), 5%V-TiO<sub>2</sub>[NTA] (400), and 1%V-TiO<sub>2</sub>[NTA] (300–800) samples recorded at room temperature in air. ESR is a highly sensitive spectroscopic technique for examining paramagnetic species and can give valuable information. From Fig. 9a, it can be seen that as-prepared NTA do not show any ESR signal, meaning that it is free of paramagnetic species. However, after as-prepared NTA was heat-treated at 400 °C for 4 h in air, the resultant catalyst sample (i.e., 0%V-TiO<sub>2</sub>[NTA] (400)) shows an intense ESR signal at  $g=2.002$ , indicating that this sample contains a certain amount of paramagnetic species. Some researchers had assigned the typical ESR spectrum of TiO<sub>2</sub> after heat-treated in vacuum to electrons trapped at oxygen-defect site, which was denoted as SETOV [33,60–62]. Our

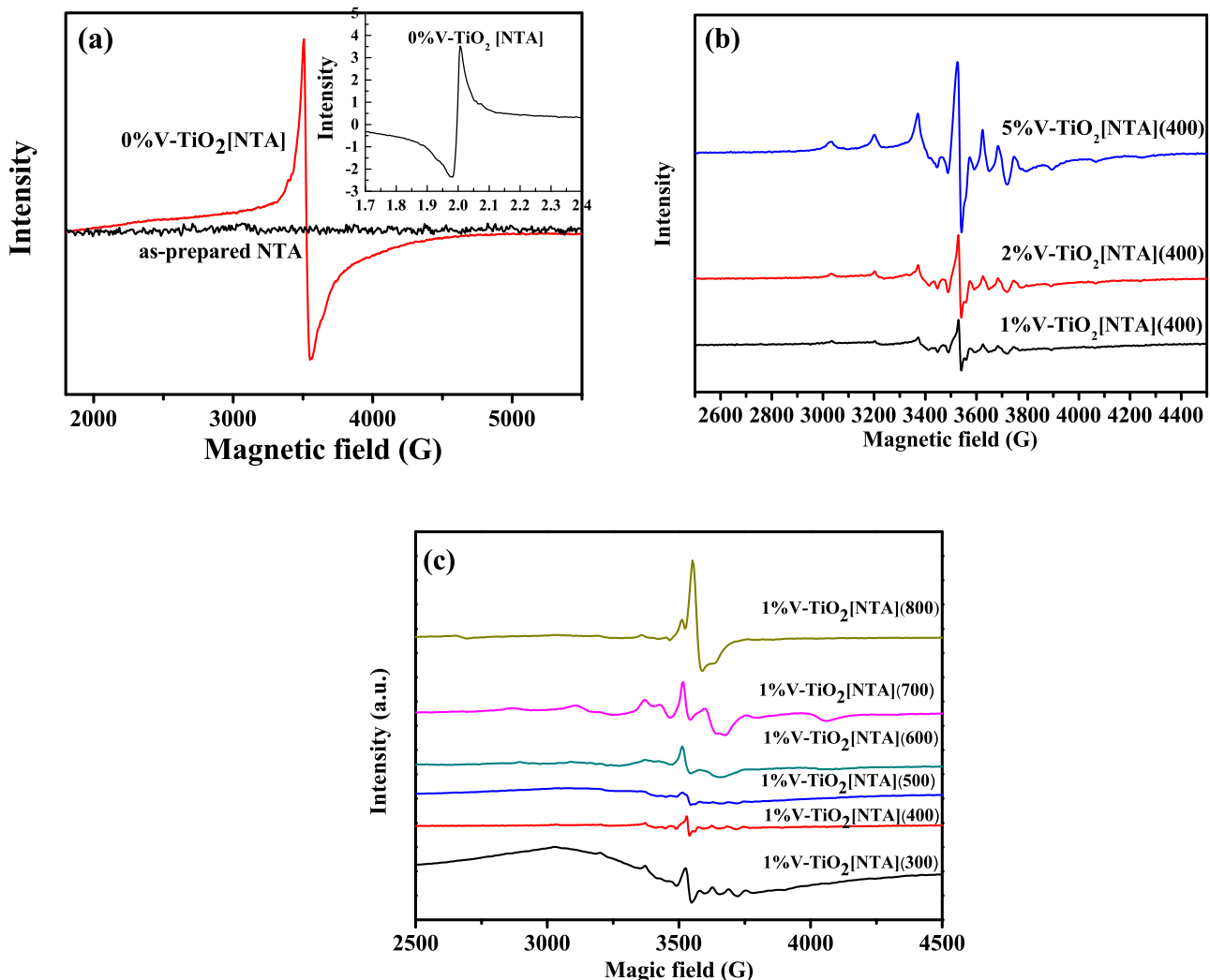


**Fig. 9.** ESR spectra of (a) as-prepared NTA and 0%V-TiO<sub>2</sub>[NTA] (400); (b) 1%V-TiO<sub>2</sub>[NTA] (400), 2%V-TiO<sub>2</sub>[NTA] (400), 5%V-TiO<sub>2</sub>[NTA] (400) and 1%V-TiO<sub>2</sub>[NTA] (500); and (c) 1%V-TiO<sub>2</sub>[NTA] (300–800). The inset of (a) is the g factor of the sample 0%V-TiO<sub>2</sub>[NTA] (400).

research group has investigated the properties of NTA prepared by hydrothermal method systematically. It is found that there is a symmetrical ESR signal at  $g = 2.003$ , which is assigned to SETOV, when NTA is either annealed in air or dehydrated in vacuum [15]. Based on the above discussions, the ESR signal observed for 0%V-TiO<sub>2</sub>[NTA] (400) is ascribed to SETOV. From Fig. 9b and c, we found that 1%V-TiO<sub>2</sub>[NTA] (400), 2%V-TiO<sub>2</sub>[NTA] (400), 5%V-TiO<sub>2</sub>[NTA] (400) and 1%V-TiO<sub>2</sub>[NTA] (500) all exhibit obvious eight-component hyperfine structure, which can be contributed to the dipole-dipole interaction between the spin magnetic moment of the <sup>51</sup>V nucleus ( $I = 7/2$ ) and the electronic spin moment of the paramagnetic V<sup>4+</sup> ions ( $S = 1/2$ ). The eight well-resolved line signals indicate that V<sup>4+</sup> ions have been incorporated into the crystal lattice to substitute Ti<sup>4+</sup> ions of TiO<sub>2</sub> matrix [56,57]. What a surprise, we do not find any paramagnetic signal of SETOV species for all V-TiO<sub>2</sub>[NTA]. Herein, V<sup>4+</sup> species was the only paramagnetic species at present. As V<sup>5+</sup> is the only vanadium precursor in NH<sub>4</sub>VO<sub>3</sub>, the SETOV produced by the intra-layered dehydration of NTA under high temperature conditions may reduce V<sup>5+</sup> to V<sup>4+</sup> during using NTA as the titanium source to synthesize V-TiO<sub>2</sub>[NTA], thus, consuming the electrons trapped at oxygen vacancy states. The V<sup>4+</sup> can be stabilized into the TiO<sub>2</sub>, whereas V<sup>5+</sup> is likely the major chemical state on the surface of the anatase catalyst [41,57]. Therefore, there are paramagnetic signal of V<sup>4+</sup> species instead of SETOV species. Moreover,

we found that the signal intensity of eight-component hyperfine structure is increased with the increase of V-doping concentration, which can be ascribed to many more intra-lattice V<sup>4+</sup> species at higher V-doping concentration, in accordance with the increased absorbance. It is worthy of our attention that the signal intensity of eight-component hyperfine structure decreased with annealing temperature, and it reached minimum at 500 °C, and then increased above 500 °C indicating an optimal amount of V<sup>4+</sup> species.

### 3.9. Calculation of density of states (DOS)

To deeply understand the experiments results observed for the V-TiO<sub>2</sub>[NTA], DFT calculations were performed. Fig. 10a shows the calculated electronic density of states (DOS) for the defect-free anatase TiO<sub>2</sub>. We obtain a band gap of about 3.0 eV, which is in good agreement with the experimental results (3.2 eV). The valence band (VB) and conduction band (CB) mainly consist of O 2p and Ti 3d states. The calculated DOS of V<sub>o</sub><sup>•</sup>-TiO<sub>2</sub> is shown in Fig. 10b. It can be seen that the impurity states have gone into the conduction band, which suggestss that V<sub>o</sub><sup>•</sup> is completely ionized and becomes free electron. This can be explained by the low ionization potentials of the SETOV. Thus, these states can facilitate the transport of the photo-generated carriers to the active sites on the surface. At the same time, localized impurity state caused by SETOV from Ti 3d

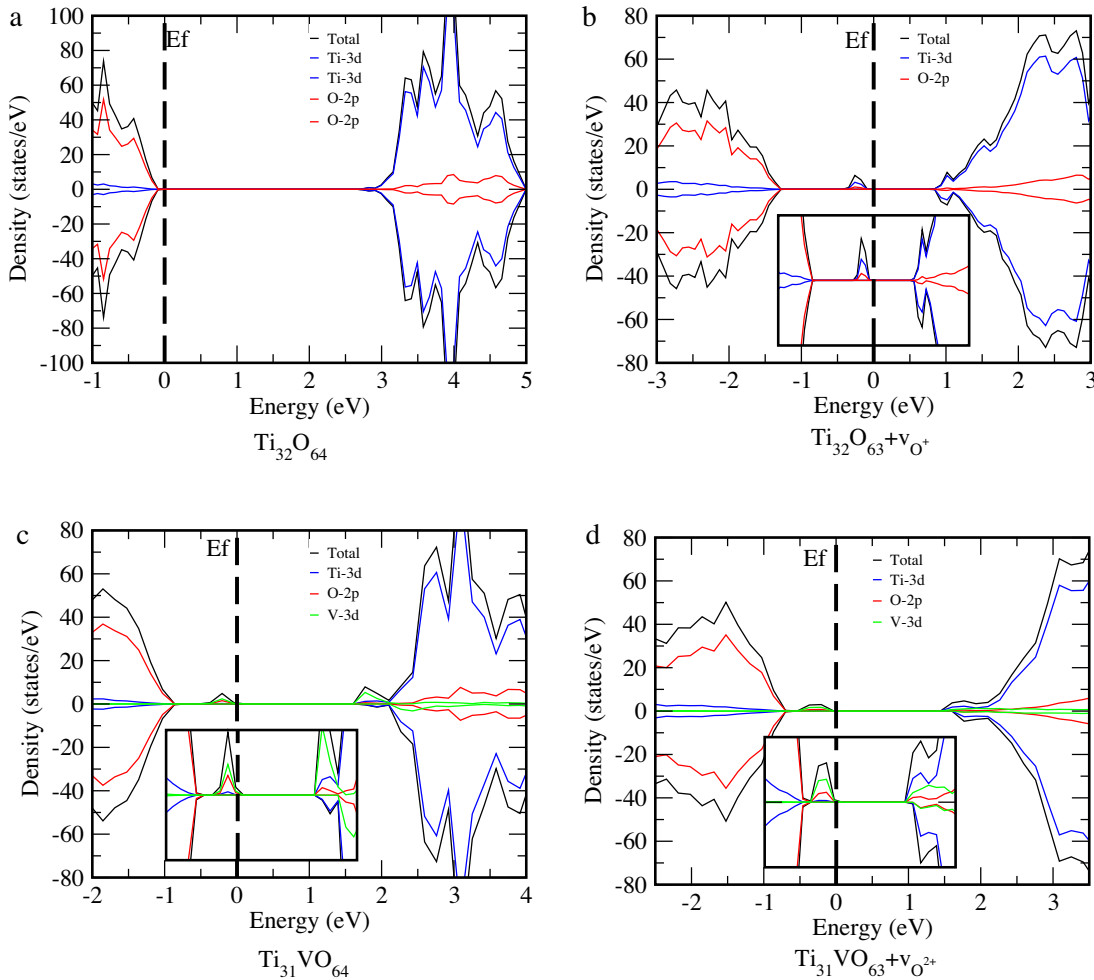


**Fig. 10.** Density of states of (a) pure  $\text{TiO}_2$ , (b)  $\text{V}_o^{\bullet}\text{-TiO}_2$ , (c)  $\text{V-TiO}_2$ , and (d)  $\text{V-V}_o^{2+}\text{-TiO}_2$ .

appears within the band gap. The visible light absorption for novel  $\text{TiO}_2$  with  $\text{V}_o^{\bullet}$  originates from this impurity state. However, its existence is unfavorable for photoactivity, because it introduces a deep donor level within band gap and readily becomes carrier recombination center, which corresponds to no observed experimental photocatalytic activity under visible light irradiation though it has visible light absorption [15–17]. For V-doped  $\text{TiO}_2$  without  $\text{V}_o^{\bullet}$ ( $\text{V-TiO}_2$ ), it can be seen from Fig. 10c that upon doping V ions into the lattice of the  $\text{TiO}_2$  crystal, several localized impurity states contributed by V 3d occur near the top of the valence band and within the band-gap as well as below the conduction band. Although the formation of these strongly localized d states can reduce the band gap of  $\text{TiO}_2$  to some extent, it also introduces a new carrier recombination center and significantly reduces carrier mobility. This can be proved by lower photocatalytic activity of 1%V-P25- $\text{TiO}_2$  (as shown in Fig. 1). The DOS of  $\text{V}+\text{V}_o^{2+}\text{-TiO}_2$  (modeled  $x\%\text{V-TiO}_2[\text{NTA}]$  (400) samples based on the observed ESR signal) were also calculated and were shown in Fig. 10d. Compared with the  $\text{V}_o^{\bullet}\text{-TiO}_2$  (Fig. 10b) and  $\text{V-TiO}_2$  (Fig. 10c), the deep donor level hybridized by the Ti 3d and O 2p states within the band gap disappeared, while the mixing states of V 3d, and O 2p above the valence band moved to the top of the valence band at 0 eV in the  $\text{V}+\text{V}_o^{2+}\text{-TiO}_2$ . At the same time, the states mainly consisted of V 3d at the bottom of the CB also disappeared, the new electronic states consisted of Ti 3d, V 3d, and O 2p appeared on the bottom of the CB in  $\text{V}+\text{V}_o^{2+}\text{-TiO}_2$ . As a result, the new states of V–O–Ti of  $\text{V}+\text{V}_o^{2+}\text{-TiO}_2$  in the band gap were largely overlapped with the band states of  $\text{TiO}_2$ . In

other words, the band gap is effectively narrowed, which favors the visible-light absorption and trapping the photoinduced carriers to prolong their lifetimes and facilitated the transfer of them. Therefore, we can conclude that the effective phtotactivity of  $x\%\text{V-TiO}_2[\text{NTA}]$  (400) should be mainly due to the synergistic effect of  $\text{V}_o^{\bullet}$  and V dopants. The presence of the new mixing states, originated from the Ti 3d, O 2p, and V 3d states in the band gap due to  $\text{V}^{4+}$  incorporated into crystal lattice of  $\text{TiO}_2$ , tends to lead to a decrease in band gap and hence are more favorable for the absorption in the visible-light region.

### 3.10. Photocatalytic activity and mechanism

The visible light photocatalytic activity of  $\text{V-TiO}_2[\text{NTA}]$  samples was evaluated by photooxidation removal of propylene. In Fig. 11a, we first investigate the effect of the amount of V doping (from 0 to 10% of V/Ti) on the removal yield of propylene. It can be seen that the doping of  $\text{TiO}_2$  with V favors the removal of propylene. However, the activity of the photocatalysts for the removal yield of  $\text{C}_3\text{H}_6$  increased with increasing of doping concentration, and it reached maximum for a level of 1% mol V, and then decreased above 1% mol V, indicating an optimal concentration of dopant and meaning that the amount of doped-V is very important to photoactivity. The results demonstrated that 1%V-TiO<sub>2</sub>[NTA] (400) exhibits the most significantly enhanced photocatalytic activity, which is approximately 12 times higher than that of pure NTA (400).

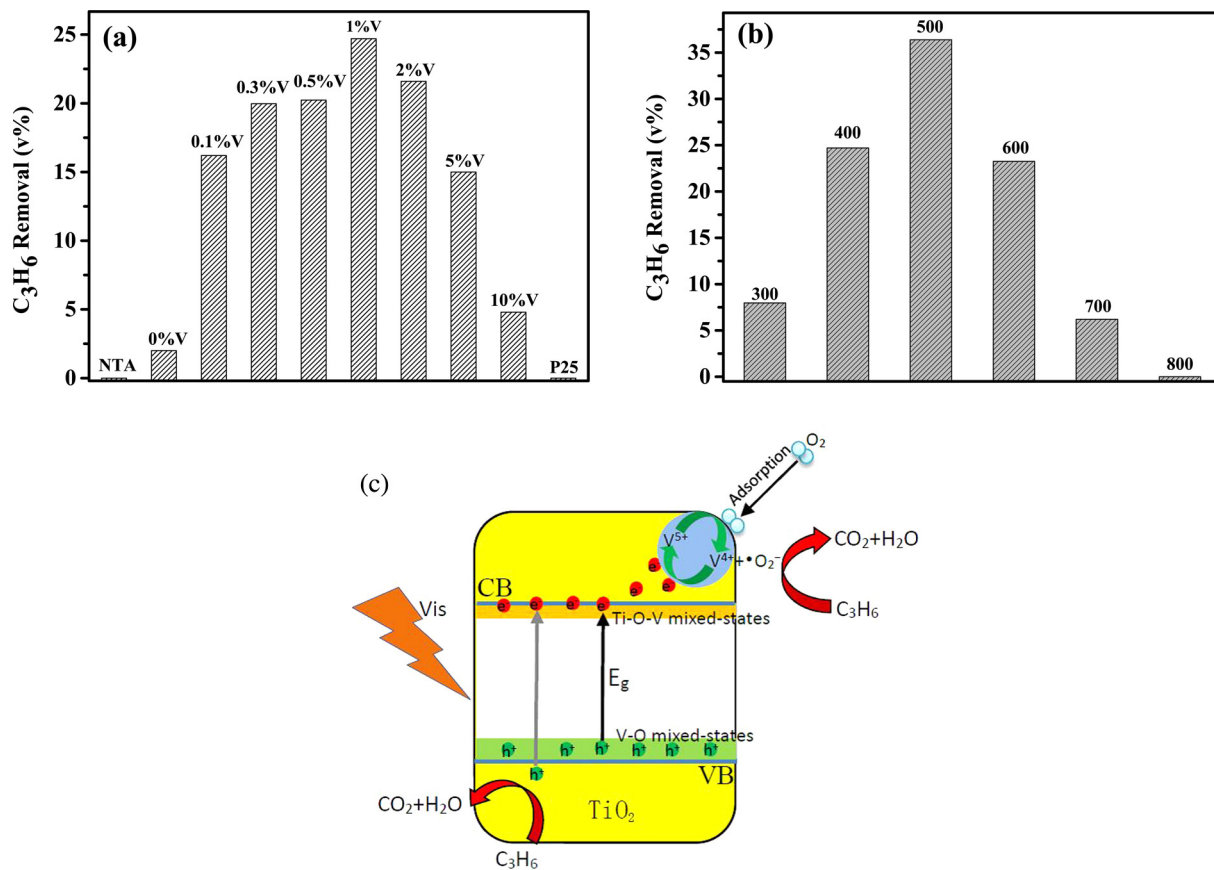


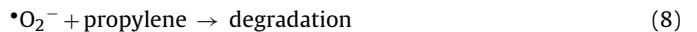
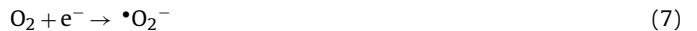
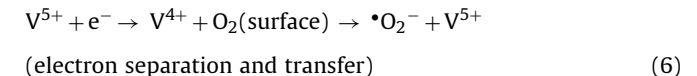
**Fig. 11.** (a) Photocatalytic degradation of propylene over as-prepared NTA, x%V-TiO<sub>2</sub>[NTA] (400), (b) photocatalytic degradation of propylene over 1%V-TiO<sub>2</sub>[NTA] annealed at 300–800 °C, and (c) schematic diagrams of the photodegradation of propylene over V-TiO<sub>2</sub>[NTA] under visible light irradiation.

On the other hand, the effect of calcination temperature on photocatalytic oxidation rate of propylene over 1%V-TiO<sub>2</sub>[NTA] samples is also investigated, as shown in Fig. 11b. When calcined temperature at 300 °C, there is a very low photocatalytic activity observed for the sample 1%V-TiO<sub>2</sub>[NTA] (300), which is due to the fact that the sample possesses the poor crystallization and large  $S_{\text{BET}}$  (334.383 m<sup>2</sup>/g). As calcination temperature is increased, photocatalytic activity reaches an optimal value at 500 °C, which can be ascribed to an obvious improvement in crystallization (Fig. 5d). With the further increasing calcination temperature, the photocatalytic activity decreases rapidly and reaches a minimum value at 800 °C which may contribute to the existence of more defect states.

It is well known that the crystalline structure and specific surface area are two important factors that influence the photocatalytic activity of TiO<sub>2</sub>. However, in this study, only little variation of crystalline structure was found for different V-TiO<sub>2</sub>[NTA] samples. Thus, the variation of photocatalytic activity of different V-TiO<sub>2</sub>[NTA] samples cannot be mainly assigned to the influences of crystalline structure. Combining on the results of the UV-vis and  $S_{\text{BET}}$  analysis, the main factor influencing the photocatalytic activity of V-TiO<sub>2</sub>[NTA] is the  $S_{\text{BET}}$  or intralattice V<sup>4+</sup> of TiO<sub>2</sub> matrix when the V concentration is below 1%. It has been reported that V dopants can influence the photocatalytic activity of TiO<sub>2</sub> by acting as trapping centers for photo-generated electron(e<sup>-</sup>) and/or hole(h<sup>+</sup>) and by altering the recombination rate of e<sup>-</sup>/h<sup>+</sup> pairs [9,36,56]. ESR spectrum show that the content of V<sup>4+</sup> increases with the increasing of V doping concentration, however, the photocatalytic activity is reduced when the V concentration is above 1%.

On the basis of the above experimental and DFT calculational results, at low concentration, the enhancement of photocatalytic activity for the V-TiO<sub>2</sub>[NTA] samples should be ascribed to the

synergistic effect of V and V<sub>0</sub><sup>•</sup> co-doping. The possible photocatalytic degradation mechanism of propylene were proposed and elucidated in Fig. 11c and Eqs. (4)–(9).



Firstly, V<sup>5+</sup> is reduced to V<sup>4+</sup> by SETOV, which is produced by heated the doping precursor and as-prepared NTA. This V<sup>4+</sup> replaces Ti<sup>4+</sup> ions in the TiO<sub>2</sub> to form continuous impurity levels from the Ti 3d, O 2p, and V 3d states above the valence band and below the conduction band, as shown in Fig. 11c, respectively. Thus, these impurity energy levels created between the VB and the CB by the incorporation of V<sup>4+</sup> dopants cause the absorption edge to shift further into visible region as compared to pure TiO<sub>2</sub>. By improving the light absorption efficiency of TiO<sub>2</sub>, a larger number of photogenerated charges can be formed (see Eq. (5)). Due to the lower Fermi level of V<sup>5+</sup> species on the surface, the photogenerated electrons in the CB may immediately transfer to V<sup>5+</sup> ions leaving back holes on the VB of TiO<sub>2</sub> resulting in the effective separation of e<sup>-</sup> and h<sup>+</sup> (see Eq.

(6)). The V<sup>4+</sup> species, created from V<sup>5+</sup> by electron trapping, easily release and transfer electron to oxygen molecule absorbed on the surface of TiO<sub>2</sub> to produce superoxide radicals •O<sub>2</sub><sup>-</sup> (Fig. 11c). O<sub>2</sub> adsorbed on the surface of the photocatalyst can only react with V<sup>4+</sup> to generate •O<sub>2</sub><sup>-</sup>. Namely, it can react with e<sup>-</sup> to generate •O<sub>2</sub><sup>-</sup> (see Eqs. (6) and (7)). Both of h<sup>+</sup> and •O<sub>2</sub><sup>-</sup> were indeed strong oxidizing agents required for the degradation of the propylene. Therefore, the presence of the V<sup>4+</sup>/V<sup>5+</sup> pair can efficiently separate the electrons and holes to generate •O<sub>2</sub><sup>-</sup> and h<sup>+</sup> for the degradation of the propylene. The same trapping sites act as the recombination centers might be the reasons of the decrease in photocatalytic activity above 1% concentration of V doping in TiO<sub>2</sub>. Moreover, excess V dopant might occupy the active sites and form low cover on the TiO<sub>2</sub> surface, which not only influences the penetration of light but also reduces the adsorptive function of organic pollutants on the surface of TiO<sub>2</sub> and the contact area between TiO<sub>2</sub> and organic pollutant. As a result, excess V concentration and high temperature leads to the decreasing of photocatalytic activity.

#### 4. Conclusions

By a facile solid state sintering method, using the nanotubular titanic acid (NTA) as titanium precursor, different concentration of the novel V-TiO<sub>2</sub>[NTA] samples have been successfully synthesized for the first time. V dopant has been successfully incorporated into the crystal lattice of TiO<sub>2</sub> in the form of V<sup>4+</sup> ions, created from V<sup>5+</sup> reduced by SETOV. At the same time, V<sup>5+</sup> ions exists on the surface in the form of V<sub>2</sub>O<sub>5</sub>. The activity of V-TiO<sub>2</sub>[NTA] in photocatalytic oxidation of propylene was evaluated under visible light irradiation. It was found that 1%V-TiO<sub>2</sub>[NTA] (500) displayed remarkable photocatalytic activity for degradation of propylene under visible-light irradiation, which is significantly better than that of as-prepared NTA, P25 TiO<sub>2</sub>, N-TiO<sub>2</sub>[NTA], and V-doped P25 TiO<sub>2</sub>. The remarkable improved photocatalytic activity of the V-TiO<sub>2</sub>[NTA] may be resulted from the synergistic effect: (i) the increased visible light absorption by the narrowing of gap originated from the appearance of new states (around the top of the valence band, due to O 2p and V 3d orbitals; around the bottom of the conduction band, due to Ti 3d, O 2p, and V 3d orbitals); (ii) the efficient separation and transfer of the photogenerated e<sup>-</sup>/h<sup>+</sup> pairs due to the presence of V<sup>5+</sup>/V<sup>4+</sup> redox couple.

#### Author contributions

F.Z. Ren and H.Y. Li are jointly responsible for designing this work, analyzing the data and writing the manuscript. The DFT calculations and the experiments examination were performed by F.Z. Ren and H.Y. Li, respectively. All authors gathered to discuss the results. Y.X. Wang and J.J. Yang decided the manuscript final version.

#### Acknowledgments

The authors gratefully acknowledge the support of Program for the National Natural Science Foundation of China (Nos. 51371076, 20973054), Excellent Doctoral Dissertation breeding program of Henan University (No. Y1317011), and Innovative Research Team (in Science and Technology) in University (Nos. 13IRTSTHN017 and PCSIRT1126).

#### References

- [1] A. Fujishima, K. Honda, *Nature* 238 (1972) 37–38.
- [2] A. Nakata, K. Fujishima, *J. Photochem. Photobiol. C: Photochem. Rev.* 13 (2012) 169–189.
- [3] S.C. Roy, O.K. Varghese, M. Paulose, C.A. Grimes, *Acs Nano* 4 (2010) 1259–1278.
- [4] M.R. Hoffmann, S.T. Martin, W. Choi, D.W. Bahnemann, *Chem. Rev.* 95 (1995) 69–96.
- [5] M. Hagfeldt, A. Graetzel, *Chem. Rev.* 95 (1995) 49–68.
- [6] M.I. Litter, *Appl. Catal. B: Environ.* 23 (1999) 89–114.
- [7] X. Chen, S.S. Mao, *Chem. Rev.* 107 (2007) 2891–2959.
- [8] H. Yamashita, H. Harada, J. Misaka, M. Takeuchi, K. Ikeue, M.J. Anpo, *Photochem. Photobiol. A* 148 (2002) 257–261.
- [9] W.Y. Choi, A. Termin, M.R. Hoffmann, *J. Phys. Chem.* 98 (1994) 13669–13679.
- [10] I. Justicia, P. Ordejon, G. Canto, J.L. Mozos, J. Fraxedes, G.A. Battiston, R. Gerbasi, A. Figueras, *Adv. Mater.* 14 (2002) 1399–1402.
- [11] R. Dholam, N. Patel, M. Adami, A. Miotello, *In. J. Hydrogen Energy* 34 (2009) 5337–5346.
- [12] S. Rehman, R. Ullah, A.M. Butt, N.D. Gohar, *J. Hazard. Mater.* 170 (2009) 560–569.
- [13] Y. Gai, J. Li, S.S. Li, J. b. Xia, S.H. Wei, *Phys. Rev. Lett.* 102 (2009) 36402–36404.
- [14] S. Livraghi, M.C. Paganini, E. Giannello, A. Selloni, C. Di Valentin, G. Pacchioni, *J. Am. Chem. Soc.* 128 (2006) 15666–15671.
- [15] M. Zhang, Z.S. Jin, J.W. Zhang, X.Y. Guo, J.J. Yang, W. Li, X.D. Wang, Z.J. Zhang, *J. Mol. Catal. A: Chem.* 217 (2004) 203–210.
- [16] Q.Y. Li, J.W. Zhang, Z.S. Jin, D.G. Yang, X.D. Wang, J.J. Yang, Z.J. Zhang, *Electrochim. Commun.* 8 (2006) 741–746.
- [17] X. Wang, J. Yang, H. Yin, Z. Zhang, Z. Jin, *Photogr. Sci. Photochem.* 20 (2002) 424–428.
- [18] Q.Y. Li, X.D. Wang, Z.S. Jin, D.G. Yang, S.L. Zhang, X.Y. Guo, J.J. Yang, Z.J. Zhang, *J. Nanopart. Res.* 9 (2007) 951–957.
- [19] Y. Wang, C.X. Feng, Z.S. Jin, J.W. Zhang, J.J. Yang, S.L. Zhang, *J. Mol. Catal. A: Chem.* 260 (2006) 1–3.
- [20] Y. Wang, C.X. Feng, M. Zhang, J.J. Yang, Z.J. Zhang, *Appl. Catal. B: Environ.* 104 (2011) 268–274.
- [21] C.X. Feng, Y. Wang, J.W. Zhang, L.G. Yu, D.L. Li, J.J. Yang, Z.J. Zhang, *J. Appl. Catal. B: Environ.* 113–114 (2012) 61–71.
- [22] Y. Wang, M.J. Jing, M. Zhang, J.J. Yang, *Catal. Commun.* 20 (2012) 46–50.
- [23] Y. Wang, X.J. Meng, X.L. Yu, M. Zhang, J.J. Yang, *Appl. Catal. B: Environ.* 138–139 (2013) 326–332.
- [24] M. Iwasea, K. Yamada, T. Kurisakia, B. Ohtanib, H. Wakitaa, *Appl. Catal. B: Environ.* 140–141 (2013) 327–332.
- [25] Y. Wang, P. Ren, C. Feng, X. Zheng, Z. Wang, D. Li, *Mater. Lett.* 115 (2014) 85–88.
- [26] N. Serpone, D. Lawless, J. Disdier, J.M. Herrmann, *Langmuir* 10 (1994) 643–652.
- [27] S. Liu, T. Xie, Z. Chen, J. Wu, *Appl. Surf. Sci.* 255 (2009) 8587–8592.
- [28] B. Tian, C. Li, F. Gu, H. Jiang, Y. Hu, J. Zhang, *Chem. Eng. J.* 151 (2009) 220–227.
- [29] M. Anpo, M. Takeuchi, *J. Catal.* 216 (2003) 505–516.
- [30] S. Klosek, D. Rafra, *J. Phys. Chem. B* 105 (2001) 2815–2819.
- [31] J.K. Zhou, M. Takeuchi, A.K. Ray, M. Anpo, X.S. Zhao, *J. Colloid Interf. Sci.* 311 (2007) 497–501.
- [32] J.C.-S. Wu, C.H. Chen, *J. Photochem. Photobiol. A: Chem.* 163 (2004) 509–515.
- [33] H. Yamashita, H. Harada, J. Misaka, M. Takeuchi, K. Ikeue, M. Anpo, *J. Photochem. Photobiol. A* 148 (2002) 257–261.
- [34] A. Kubacka, A. Fuerte, A. Martinez-Arias, M. Fernandez-Garcia, *Appl. Catal. B: Environ.* 74 (2007) 26–33.
- [35] X. Yang, F. Ma, K. Li, Y. Guo, J. Hub, W. Li, M. Huo, Y. Guo, *J. Hazard. Mater.* 175 (2010) 429–438.
- [36] R. Jaiswala, N. Patelb, D.C. Kotharia, A. Miotello, *Appl. Catal. B: Environ.* 126 (2012) 47–54.
- [37] R. Dholam, N. Patel, A. Miotello, *In. J. Hydrogen Energy* 36 (2011) 6519–6528.
- [38] Y. Nakano, T. Morikawa, T. Ohwaki, Y. Taga, *Appl. Phys. Lett.* 86 (2005) 132104–132113.
- [39] K. Bhattacharyya, S. Varma, A.K. Tripathi, S.R. Bharadwaj, A.K. Tyagi, *J. Phys. Chem. C* 112 (2008) 19102–19112.
- [40] K. Bhattacharyya, S. Varma, A.K. Tripathi, S.R. Bharadwaj, A.K. Tyagi, *J. Phys. Chem. B* 113 (2009) 5917–5928.
- [41] A. Vittadini, M. Casarin, M. Sambi, A. Selloni, *J. Phys. Chem. B* 109 (2005) 21766–21771.
- [42] B. Schimmoeller, H. Schulz, A. Ritter, A. Reitzmann, B. Kraushaar-Czernetzki, A. Baiker, S.E. Pratsinis, *J. Catal.* 256 (2008) 74–83.
- [43] F. Trifirò, *Catal. Today* 41 (1998) 21–35.
- [44] J.-M. Herrmann, J. Disdier, G. Deo, I.E. Wachs, *J. Chem. Soc., Faraday Trans. 93* (1997) 1655–1660.
- [45] G. Kresse, J. Hafner, *Phys. Rev. B* 47 (1993) 558–561.
- [46] G. Kresse, J. Furthmüller, *Phys. Rev. B* 54 (1996) 11169–11186.
- [47] Y. Perdew, J.P. Wang, *Phys. Rev. B* 45 (1992) 13244–13249.
- [48] J.P. Perdew, K. Burke, M. Ernzerhof, *Phys. Rev. Lett.* 77 (1996) 3865–3868.
- [49] P. Blchl, *Phys. Rev. B* 50 (1994) 17953–17979.
- [50] K.S. Yang, Y. Dai, B.B. Huang, *ChemPhysChem* 10 (2009) 2327–2333.
- [51] I. Solov'yev, N. Hamada, K. Terakura, *Phys. Rev. B* 53 (1996) 7158–7162.
- [52] C.G. Van de Walle, J. Neugebauer, *J. Appl. Phys.* 95 (2004) 3851–3879.
- [53] X. Ma, Y. Wu, Y. Lu, J. Xu, Y. Wang, Y. Zhu, *J. Phys. Chem. C* 115 (2011) 16963–16969.
- [54] L. Li, C. Liu, Y. Liu, *Mater. Chem. Phys.* 113 (2009) 551–557.
- [55] (a) S. Rajeshkumar, C. Suresh, A.K. Vasudevan, N.R. Suja, P. Mukundan, K.G.K. Warrier, *Mater. Lett.* 38 (1999) 161–166;
- (b) S. Rajeshkumar, C. Suresh, A.K. Vasudevan, P. Perumal, K.G.K. Warrier, *Trans. Ind. Ceram. Soc.* 58 (1999) 118;
- (c) D. Vorkapic, T. Matscuks, *J. Am. Ceram. Soc.* 81 (1998) 2815–2820;
- (d) H. Zhang, J.F. Banfield, *J. Mater. Res.* 15 (2000) 437;

- (e) C.P. Sibu, S.R. Kumar, P. Mukundan, K.G.K. Warrier, *Chem. Mater.* 14 (2002) 2876–2881.
- [56] B. Tiana, C. Li, F. Gua, H. Jiang, Y. Hua, J. Zhang, *Chem. Eng. J.* 151 (2009) 220–227.
- [57] J. Liu, R. Han, Y. Zhao, H. Wang, W. Lu, T. Yu, Y. Zhang, *J. Phys. Chem. C* 115 (2011) 4507–4515.
- [58] Y. Wang, Y. Huang, W.K. Ho, L.Z. Zhang, Z.G. Zou, S.C. Lee, *J. Hazard. Mater.* 169 (2009) 77–87.
- [59] C.C. Wang, K.W. Wang, T.P. Perng, *Appl. Phys. Lett.* 96 (2010) 143102-1–143102-3.
- [60] X. Zou, J. Liu, J. Su, F. Zuo, J. Chen, P. Feng, *Chem. Eur. J.* 19 (2013) 2866–2873.
- [61] Y.B. Jiang, W.B. Mi, E.Y. Jiang, H.L. Bai, *J. Vac. Sci. Technol. A* 27 (2009) 1172–1177.
- [62] A.R. Albuquerque, A. Bruix, I.M.G. dos Santos, J.R. Sambrano, F. Illas, *J. Phys. Chem. C* 118 (2014) 9677–9689.